Toxicology Research

Accepted Manuscript

ROYAL SOCIETY OF CHEMISTRY

www.rsc.org/toxicology

The acute hepatotoxicity of tacrine explained by ^{1}H NMR based metabolomic profiling

Yan-Hong Lou [a], Jun-Song Wang [b*], Ge Dong [a], Ping-Ping Guo [a], Dan-Dan Wei [a], Sai-Sai Xie [a], Ming-Hua Yang [a], Ling-Yi Kong [a*]

[a] State Key Laboratory of Natural Medicines, Department of Natural Medicinal Chemistry, China Pharmaceutical University, 24 Tong Jia Xiang, Nanjing, 210009, People's Republic of China

[b] Center for Molecular Metabolism, Nanjing University of Science and Technology, 200 Xiao Ling Wei Street, Nanjing, 210094, People's Republic of China

***Corresponding authors: Prof. Lingyi Kong and Prof. Junsong Wang**

Tel/Fax: +86 25 8327 1405 (Lingyi Kong); Tel: +86 25 8431 5512 (Junsong Wang)

E-mail: cpu_lykong@126.com (Lingyi Kong); wang.junsong@gmail.com (Junsong Wang)

Abstract

Tacrine is a well-known acetylcholinesterase inhibitor used for the treatment of Alzheimer's disease (AD). Unfortunately, occurrence of hepatotoxicities was found in about 30% of patients taking tacrine at its therapeutic doses, which severely limits its clinical use. The mechanism of its hepatotoxicity has not been fully elucidated. The purpose of this study was to develop and characterize a model of acute hepatotoxicity induced by tacrine to understand the mechanism by ^{1}H NMR based metabolomics approach. Rats were first intraperitoneally injected with tacrine solution (11.89 mg/kg body weight). Histopathological inspections at 24 hours after treatment with tacrine disclosed severe liver damage. In addition, the activities of enzymes and the expressions of relevant genes were measured in this study. An orthogonal signal correction partial least-squares discriminant analysis (OSC-PLSDA) of the metabolomic profiles of rat liver tissues highlighted a number of metabolic disturbances induced by tacrine, focusing on energy metabolism and oxidative stress. These findings could well explain tacrine-induced acute hepatotoxicity and reveal several potential biomarkers associated with this toxicity. This integrated metabolomics approach demonstrated its feasibility and allowed better understanding of tacrine-induced liver toxicity dynamically and holistically.

1 Introduction

Alzheimer's disease (AD) is a progressive, degenerative dementia characterized by decreased cognitive functions with associated decline in cholinergic transmission.[1]

With the ageing of the world population, the prevalence, cost, societal burden of AD and the importance to development therapeutics for this devastating disease are getting increased. Increase of cholinergic transmission is one strategy to ameliorate the symptoms of AD.[2,3] Tacrine (1,2,3,4-tetrahydro-9-aminoacridine) is the first agent approved by the Food and Drug Administration for the treatment of AD and has been widely used in clinic.[4,5] Tacrine acts as an acetylcholinesterase inhibitor blocking the degradation of acetylcholine in neurons of the cerebral cortex thereby increasing cholinergic transmission.[6,7] The action of acetylcholine is terminated by its rapid hydrolysis to choline and acetic acid by acetylcholinesterase. Tacrine binds near the catalytically active site of acetylcholinesterase to inhibit its activity and thereby prolong cholinergic activity. In view of the profound cholinergic defects in AD, enhancement of cholinergic activity is thought to be the main treatment mechanism of tacrine and other similar acetylcholinesterase inhibitors.[8] Unfortunately, tacrine has been reported to induce reversible increases in serum transaminase activity like alanine aminotransferase (ALT), suggestive of hepatic injury in 30-50% of the patients.[9-12] However, the mechanism underlying the hepatotoxicity of tacrine has not been fully understood. Several studies reported that the hepatotoxicity of tacrine was due to the formation of 1-, 2-, 4- and 7-hydroxytacrine from tacrine by the catalysis of CYP1A2.[13,14] However, most observations do not support this hypothesis because tacrine has been found to be equally cytotoxic to rat hepatocytes and to HepG2 human hepatoma cells, known to lack CYP1A2 activity, and that its toxicity is not prevented by the presence of CYP1A2 inhibitors. Tacrine could induce mitochondrial

dysfunction[15,16] which, however, might not be the only factor involved since that the clinical manifestations of tacrine did not resemble those typically associated with mitochondrial cytopathies.[17]

Besides traditional means for toxicological studies, newly arising "-omics" technologies have been used, such as metabolomics.[18,19] As one component of systems biology, metabolomics concerns with the detection, identification, quantitation and differentiation of dynamic metabolic changes of living systems facing a pathological event or subjects to genetic modifications.[20,21] Nowadays, it has been widely applied in the fields of toxicity screening, disease diagnosis, drug safety assessment and mechanism study, and toxicology.[22,23] The application of metabolomics approach in toxicological studies has conspicuous superiority to traditional techniques, due to its potential to dynamically monitor and globally evaluate the response of biosystem and biological effects from the metabolic profiles.[24]

In this study, an acute toxicity of tacrine rat model was established through the intraperitoneal injection of tacrine (11.89 mg/kg), and liver samples were collected at 24 and 72 h after dosing for NMR recording. A ^{1}H NMR-based metabolomics approach combined with pattern recognition techniques was adopted to investigate the acute hepatotoxicity of tacrine on rats.

2 Materials and methods

2.1 Chemicals and reagents

Tacrine was synthesized in our laboratory with a purity of 99.8% determined by HPLC. Kits for blood aspartate aminotransferase (AST) and alanine aminotransferase (ALT), liver tissues malondialdehyde (MDA), glutathione (GSH), pyruvate kinase (PK), creatine kinase (CK) and total proteins were purchased from Nanjing Jiancheng Bioengineering Institute (Nanjing, China). Deuterium oxide (D_2O, 99.9%), sodium 3-trimethylsilyl-1-(2,2,3,3-$2H_4$) propionate (TSP), diethy pyrocarbonate and Tris were purchased from Sigma Chemical Co. (St Louis, MO, USA). Acetonitrile, chloroform, isopropanol and ethanol were bought from Shanghai Lingfeng Chemical Reagent Co., Ltd. (Shanghai, China). All reagents were of analytical grade.

2.2 Animals and Drug administration

A total of forty-four male Sprague-Dawley rats (280 ± 20 g) were bought from the Comparative Medicine Centre of Yangzhou University (Yangzhou, China). All the animals were reared in stainless steel wire-mesh cages in a well-ventilated room at a temperature of 25 ± 2 ºC and a relative humidity of 50 ± 10%, with a 12/12-h light/dark cycle. The studies were approved by the Animal Ethics Committee of the China Pharmaceutical University, and were in compliance with the National Institute of Health (NIH) guidelines for the Care and Use of Laboratory Animals.

The rats were acclimatized for 10 days with free access to food and water. After acclimatization, the rats were randomly divided into three groups. Twenty-nine rats received a single intraperitoneal (i.p.) injection of tacrine in phosphate buffer (pH 7.0) at a dosage of 11.89 mg/kg, and the remained fifteen rats as the control group, which

received equal volume of phosphate buffer.

2.3 Sample collection

At 24 and 72 h after tacrine treatment, blood samples were taken from the ocular vein of rats into tubes after 12 h fasting. Serum samples were obtained by centrifugation (14,000 × g, 10 min, 4 ºC), and stored at -80 ºC before testing the enzymatic activities of AST and ALT. The twenty-nine tacrine administrated animals were fasted overnight and sacrificed after anesthetization by chloral hydrate (300 mg/kg, i.p.) at 24 (n = 14) and 72 h (n = 15). The livers were quickly removed, flushed with ice-cold phosphate buffer solution, and then weighed. A section of the livers were fixed in 10% neutral-buffered formalin and embedded in paraffin. Serial sections of 4 μm thickness were cut from tissue blocks and stained with hematoxylin eosin (HE). All livers were stored at -80 ºC before mRNA and NMR analysis.

2.4 Biochemical parameters

Levels of MDA, GSH, PK, CK and total proteins in liver tissues, as well as activities of blood AST, ALT were analyzed with commercial kits according to the manufacturers' specification.

2.5 Quantitative real-time RT-PCR

Liver tissues mRNA extraction was performed using the RNAiso Plus reagent (TaKaRa Biotechnology Co., Ltd, Dalian, China) according to the manufacturer's

protocol. The quantitative real-time polymerase chain reaction (qRT-PCR) was performed with the LightCycler 480 (Roche Molecular Biochemicals, Mannheim, Germany).[25] The relative expression level of each gene was normalized to that of *β*-actin. The primer pairs for PCR are listed in Table 1.

Table 1 Primers used for real-time PCR assays performed on the LC480 system

Genes	Forward primer (5'-3')	Reverse primer (5'-3')
Complex I	TGGCATGCAAATCCCTCGAT	CCAGCCCTTCATAACAGGCA
Complex II	ACATCCACCTGTCACCAAGC	GCAGCCAGAGAGTAGTCCAC
CS	ACCATGACGGTGGCAATGTA	TGGTTTGCTAGTCCATGCAGA
KGDH	AGGAGACAGGTATTTGTGGAAGG	CAGGTGCAGAATAGCACCGA
GP	AAGTTCGGCTCCAAGGATGG	ATCCTCATCAGCTCCGGGAT
GS	ACAACGAGCGAGTTGGGAT	TGAGGGGAAGAGCGTGAATG

Complex I: NADH: ubiquinone oxidoreductase; Complex II: Succinate: ubiquinone oxidoreductase; CS: citrate synthase; KGDH: *α*-ketoglutarate dehydrogenase; GP: glycogen phosphorylase; GS: glutathione synthetase.

2.6 Sample preparation for ^{1}H NMR analysis

Rat livers were weighted, homogenized with an icy cold solution of acetonitrile/H_2O (1:1, v/v), and centrifuged at 14,000 × g for 10 min at 4 ºC. The upper aqueous layer of each sample was transferred into fresh tubes, and then frozen and lyophilized until dryness on a vacuum concentrator. The dried samples were dissolved in 600 μL 99.8% D_2O phosphate buffer (0.2 M Na_2HPO_4 and 0.2 M NaH_2PO_4, pH 7.0) containing 0.05% (w/v) TSP. After vortexing and centrifugation to remove any debris, the supernatant was then transferred into a 5 mm NMR tube for ^{1}H NMR analysis. D_2O was used for field frequency locking and phosphate buffer was

152 added to minimize the chemical shift variation due to pH discrepancy.

153

154 **2.7 ^{1}H NMR spectroscopy**

155 All ^{1}H NMR spectra were recorded at 25 ºC on a Bruker AV 500 MHz
156 spectrometer. For all samples, the Nuclear Overhauser Effect
157 Spectroscopy-presaturation pulse sequence (NOESYPR) was applied to suppress the
158 residual water signal. Free induction delays (FIDs) were collected with 128 transients
159 into 32 K data points, using a spectral width of 10000 Hz, with an acquisition time per
160 scan of 2.54 s, recycle delay of 2 s and a mixing time (tm) of 100 ms. All the spectra
161 were manually phased and baseline corrected using TOPSPIN software (version 3.0,
162 Bruker Biospin, Germany).

163

164 **2.8 Data processing and analysis**

165 The spectra for all samples were manually phased and baseline corrected, and
166 referenced to TSP (^{1}H, δ 0.00), using Bruker Topspin 3.0 software (Bruker GmbH,
167 Karlsruhe, Germany). The ^{1}H NMR spectra were automatically exported to ASCII
168 files using MestReNova (Version 6.1.0, Mestrelab Research SL), which were then
169 imported into "R" (http://cran.r-project.org/), and aligned with an in-house developed
170 R-script. Univariate analysis was used to assess the integration area of metabolites
171 over time and among groups using "R". The region of 4.2-5.0 ppm belonging to the
172 residual water signals was removed. The one-dimensional (1D) spectra were
173 converted to a format appropriate for statistical analysis by automatically segmenting

each spectrum into an average of 0.01 ppm integrated spectral regions (buckets) between 0.2 and 10.0 ppm using adaptive binning. The spectra were probability quotient normalized to account for different dilutions of the samples.[26] All data were mean-centered and pareto-scaled before orthogonal signal correction partial least-squares discriminant analysis (OSC-PLSDA) was carried out. Each OSC-PLSDA model was validated by repeated two-fold cross-validation; the validity of models against overfitting was assessed by the parameter R^2Y, and the predictive ability was described by Q^2Y. High Q^2Y values indicated that the differences between the groups were significant. The overfitting cannot always be detected through cross-validation, but it can be detected using permutation tests.[27-29] Permutation testing is based on the comparison of the predictive capabilities of a model using real class assignments to a number of models calculated after random permutation of the class labels. The performance measures were plotted on a histogram for visual assessment (Fig. 1). An empirical *P*-value is often calculated by determining the number of times the permutated data yielded a better result than the one using the original labels. The calculated *P*-values for permutation testing were all less than 0.05, thus confirming the validity of the OSC-PLSDA models. Classification performance was evaluated by receiver operating characteristic (ROC) plots generated using the R-package ROCR[30] (http://rocr.bioinf.mpi-sb.mpg.de). The area under the ROC curve (AUROC) was calculated, which was an indicator of the power of the constructed model. Data were expressed as mean ± SD and $P < 0.05$ was considered statistical significant. The assigned metabolites, their fold change values at 24 and 72 h after

196 tacrine treatment vs. NC, and the associated *P* values were summarized in Table 2.

197 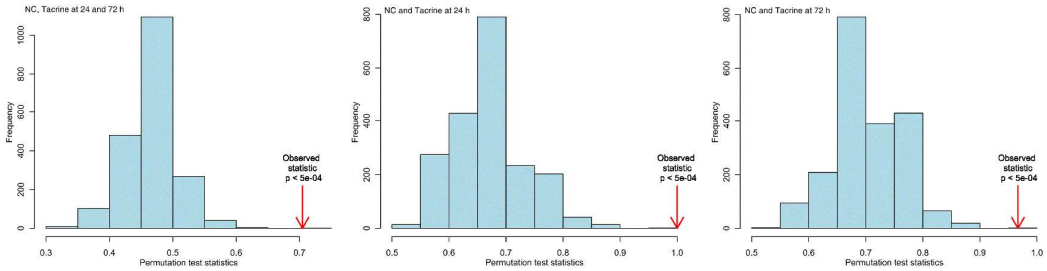

198 **Fig. 1** Histograms for permutation test scores of OSC-PLSDA models of the liver at 24 and 72
199 hours after tacrine administration on the basis of 2000 permutations: the red arrows denote the
200 performance based on the original labels. The *P*-values were all less than 0.05.

201

202 **2.9 Assignments of metabolites**

203 Resonances of metabolites were assigned by quering publicly accessible
204 metabolomics databases such as Human Metabolome Database (HMDB,
205 http://www.hmdb.ca), Madison-Qingdao Metabolomics Consortium Database
206 (MMCD, http://mmcd.nmrfam.wisc.edu/), and E. Coli Metabolome Database
207 (ECMDB, http://www.ecmdb.ca/), aided by Chenomx NMR suite 7.5 (Chenomx Inc.,
208 Edmonton, Canada) and statistical total correlations spectroscopy (STOSCY)
209 technique.[31] Metabolic pathway analysis (MetPA) was performed by Metaboanalyst
210 (http://www.metaboanalyst.ca)[32,29] to help reveal disturbed metabolism.

211

212 **3 Results**

213 **3.1 Effects of tacrine on behavior and histopathology**

214 During the experiments, symptoms such as *alvi profluvium* and bradykinesia were
215 observed among tacrine treated rats. Livers were HE stained for histopathological
216 inspection. In livers from the tacrine-treated rats at 24 h, severe cell necrosis were

detected in midzonal and pericentral regions of the liver lobule accompanied with inflammatory infiltration of portal canal, and local cells exhibited nuclear fragmentation. At 72 h, the livers of dosed rats presented moderate capsule cell necrosis, slight inflammatory cell infiltration and fiber cell hyperplasia, which suggested that liver tissues had slowly recovered at 72 h. (Fig. 2).

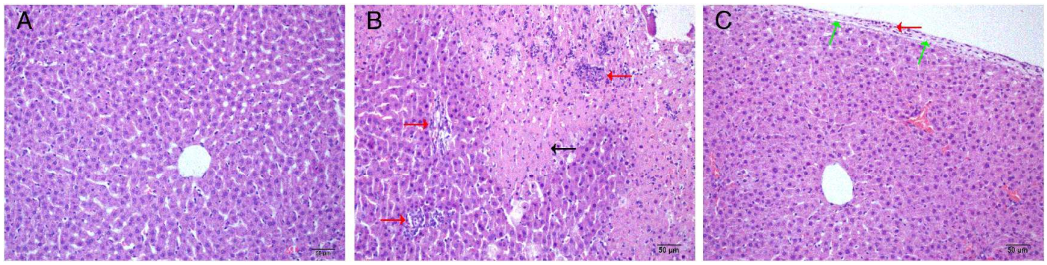

Fig. 2 Histopathological examination of control and tacrine treated liver tissues by HE staining. (A) Control rats with normal liver. (B) Liver of tacrine treated rats at 24 h group showing severe epithelial necrosis (black arrow) and cell inflammatory infiltrated (red arrow). (C) Liver of tacrine treated rats at 72 h group showing slight inflammatory cell infiltration and fiber cell hyperplasia (green arrow).

3.2 Effects of tacrine on clinical chemistry

Tacrine caused significant increase in enzyme activities of serum AST and ALT immediately at 24 h ($P < 0.001$), which were then decreased to normal levels at 72 h (Fig. 3A, 3B). These two enzymes are normally localized in the liver cytoplasm and are released into circulation after liver damages.[33] Therefore, the significantly increased levels of serum AST and ALT at 24 h confirmed hepatic injuries. The decrease of AST and ALT at 72 h suggested the recovery of livers. The responses of GSH (Fig. 3C) and total proteins (Fig. 3E) to tacrine dosing, however, were delayed: significantly increased for GSH and decreased for total proteins at 72 h but without

apparent change at 24 h. MDA (Fig. 3D) levels showed a markedly ever-increasing trend after the treatment of tacrine. Essential for glycolysis,[34] pyruvate kinase (PK) catalyzes the final step in glycolysis to convert phosphoenolpyruvate (PEP) and ADP to pyruvate and ATP. Creatine kinase (CK) catalyzes the reversible phosphorylation of creatine by ATP. The activities of PK and CK were elevated at 24 and 72 h after tacrine administration (Fig. 3F, 3G).

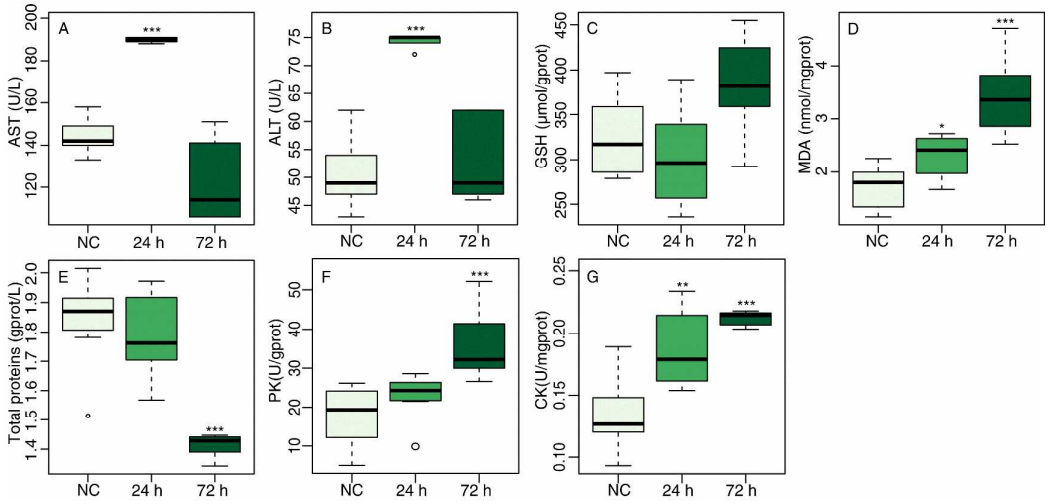

Fig. 3 Boxplots for serum levels of AST (A) and ALT (B) and liver tissue levels of GSH (C), MDA (D), total proteins (E), PK (F) and CK (G) at 24 and 72 hours after drug dosing. The bottom of each box, the line drawn in the box and the top of the box represented the 1st, 2nd and 3rd quartiles, respectively. The whiskers extended to ± 1.5 times the interquartile range (from the 1st to 3rd quartile). Outliers were shown as open circles. All values were mean ± SD (n = 7). **P* < 0.05, ***P* < 0.01 and ****P* < 0.001 vs. NC.

3.3 Effects of tacrine on the expressions of relevant genes

The hepatic expressions of NADH: ubiquinone oxidoreductase and succinate: ubiquinone oxidoreductase (Complex I and II, the components of the respiratory chain) genes were determined. At 24 h after tacrine treatment, their expressions were

significantly augmented, and then decreased at 72 h (Fig. 4A, 4B), which suggested an acceleration of the respiratory chain at 24 h induced by tacrine. Citrate synthase (CS) and α-ketoglutarate dehydrogenase (KGDH) were the key regulators of the tricarboxylic acid (TCA) cycle. The expressions of CS and KGDH genes were increased at 24 h after tacrine dosing which suggested an enhanced TCA cycle (Fig. 4C, 4D). Glycogen phosphorylase (GP) is the rate-limiting enzyme of glycogenolysis. The markedly upregulated expression of GP target gene at 24 h after tacrine treatment indicated an accelerated degradation of glycogen (Fig. 4E). Glutathione synthetase (GS) catalyzes the synthesis of GSH. The expression of GS gene was only slightly increased at 24 h after tacrine dosing, but without statistical significance (Fig. 4F). Interestingly, the expressions of these genes were significantly lower at 72 h after tacrine treatment than those of control group and 24 h group, which indicated a self-adaptive mechanism of the body to tacrine dosing.

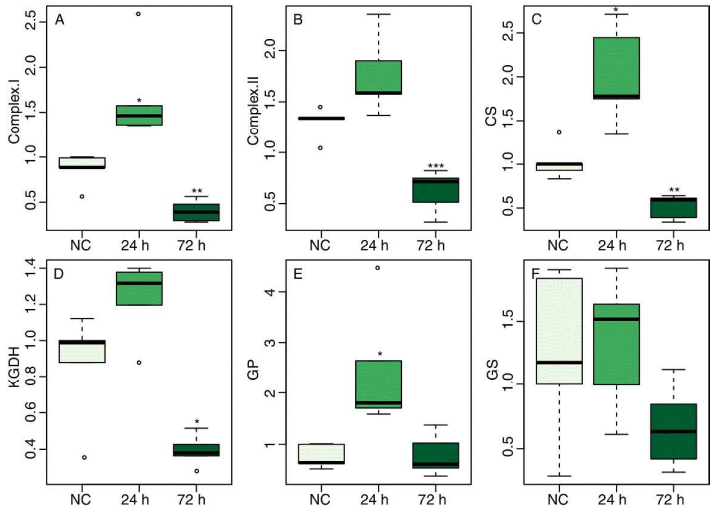

Fig. 4 Boxplots for the mRNA expression analysis by RT-PCR in livers of control group (NC) and tacrine treated groups at 24, 72 hours after dosing: (A) Complex I, (B) Complex II, (C) CS, (D) KGDH, (E) GP, (F) GS. Results of quantitative analysis values were expressed as mean ± SD (n = 5). *$P < 0.05$, **$P < 0.01$ and ***$P < 0.001$ vs. NC.

3.4 STOCSY

2D-STOCSY was used to identify correlations between spectral resonances of interest to assist in metabolite identification. Resonances arising from the same molecules are highly correlated (correlation coefficient r = 1 theoretically), which could help the elucidation of metabolites and resolve the ambiguous peaks due to overlapping. For example, strong correlations between δ 2.14 (m) and δ 2.42 (t) helped the assignment of glutamine, and the marked correlation between the signal at 2.04 ppm to that at 2.34 ppm made the assignments of them to glutamate. The resonance at 2.52 ppm had STOCSY correlation with that at 2.99 ppm, and therefore, they were assigned to isocitrate. The strong correlations between δ 9.14 (d) and δ 9.33 (s) allowed the assignment of NAD^+ (Fig. 5).

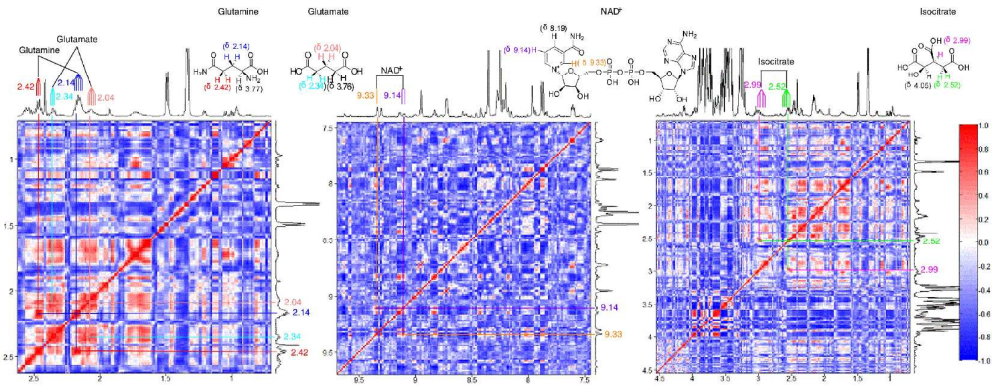

Fig. 5 Two-dimensional STOCSY analysis of liver extraction regions from 1.7 ppm to 4.0 ppm used to identify peaks of glutamine, glutamate and isocitrate, and regions from 7.5 ppm to 9.5 ppm used to identify NAD^+. The degree of correlation across the spectrum has been color coded and projected on the spectrum. The STOCSY enabled the assignments of these four metabolites as glutamine, glutamate, isocitrate and NAD^+, respectively.

3.5 Multivariate analyses of ^{1}H NMR spectra

Liver metabolic profiles were examined by OSC-PLSDA. The color-coded loading/S-plots were used to identify significantly altered metabolites. In loading plots, the significances for metabolites contributing to the class differentiation were color colored according to the absolute value of correlation coefficients. Considering both the covariance and correlation, S-plots were also generated to further identify differential markers between classes. In S-plots, the significant metabolites increased in the tacrine treated groups were in the higher-left quadrant and the decreased in the lower-right quadrant. The further away from the center of the S-plot, the more significant contribution of the metabolite to the clustering in the scores plot.

3.5.1 ^{1}H NMR spectra of livers

The typical ^{1}H NMR spectra for liver samples from control and tacine treated groups were presented in Fig. 6 with major metabolites labeled. The OSC-PLSDA analysis (R^2Y of 0.95 and Q^2Y of 0.80) of liver samples in all groups achieved a clear separation among the three groups in the scores plot (Fig. 7A), where the 24 h tacrine treated group was the furthest away from the NC group with the 72 h tacrine treated group in between, suggesting severe metabolic perturbations induced by tacrine at 24 h and also an adaptation of the body to tacrine dosing at 72 h. OSC-PLSDA analysis of NMR data for the NC group and 24 h tacrine treated group revealed a well-separation between the two groups in the scores plot (Fig. 7E). In the color coded loading plots (Fig. 7F, 7H) and S-plot (Fig. 7G), metabolites in the negative region

were elevated in the 24 h tacrine treated group: 3-hydroxybutyrate, acetate, pyruvate, glutamate, glutamine, isocitrate, dimethyl sulfone, choline/phosphocholine (Ch/PCh), trimethylamine *N*-oxide (TMAO), betaine, uridine, maleate, fumarate, xanthine, hypoxanthine, NAD^+ and $NADP^+$, while those in the positive region were reduced: taurine, glucose and glycogen. The scores plot presented marked separation of the NC group and 72 h tacrine treated group (Fig. 6I), but without apparent metabolites change (Fig. 6J, 6L and 6K).

A repeated 2-fold cross-validation method (2CV) was used to validate the statistical significance of constructed models in order to assess the risk of overfitting. The values of R^2 (explained variance of outcomes) and Q^2 (predictive ability of the model) were calculated based on a 200 times permutation test and visualized in scatter plots (Fig. 8A, 8B). The values of AUROC for the NC group and the 24 h tacrine treated group, and the NC group and the 72 h tacrine treated group were 1.000 and 0.984 respectively (Fig. 8C, 8D), showing the satisfactory classifier performance of the OSC-PLSDA model.

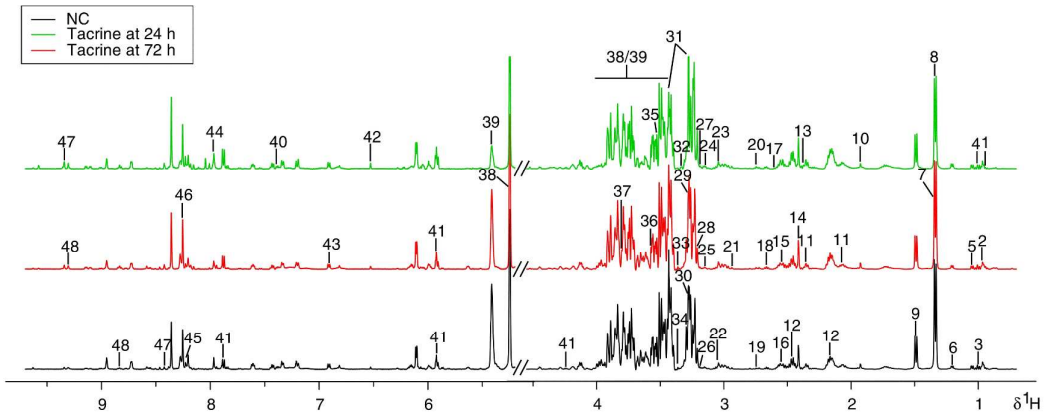

Fig. 6 Typical 500 MHz NOESYPR ^{1}H NMR spectra for the liver tissue samples from rats of the NC group and tacrine treated groups at 24 and 72 h after dosing. Metabolites: 1, isoleucine; 2,

leucine; 3, valine; 4, butanone; 5, isobutyrate; 6, 3-hydroxybutyrate; 7, 2-hydroxyisobutyrate; 8, lactate; 9, alanine; 10, acetate; 11, glutamate; 12, glutamine; 13, pyruvate; 14, succinate; 15, isocitrate; 16, *β*-alanine; 17, methylamine; 18, 5,6-dihydrouracil; 19, sarcosine; 20, dimethylamine; 21, *N*-methylhydantoin; 22, creatine/phosphocreatine (Cr/PCr); 23, creatinine; 24, malonate; 25, ethanolamine; 26, *N*-nitrosodimethylamine; 27, dimethyl sulfone; 28, choline/phosphocholine (Ch/PCh); 29, trimethylamine *N*-oxide (TMAO); 30, betaine; 31, taurine; 32, 1,3-dimethylurate; 33, caffeine; 34, methanol; 35, *S*-sulfocysteine; 36, glycine; 37, guanidoacetate; 38, glucose; 39, glycogen; 40, phenylalaine; 41, uridine; 42, fumarate; 43, protocatechuate; 44, xanthine; 45, hypoxanthine; 46, oxypurinol; 47, NAD; 48, NADP.

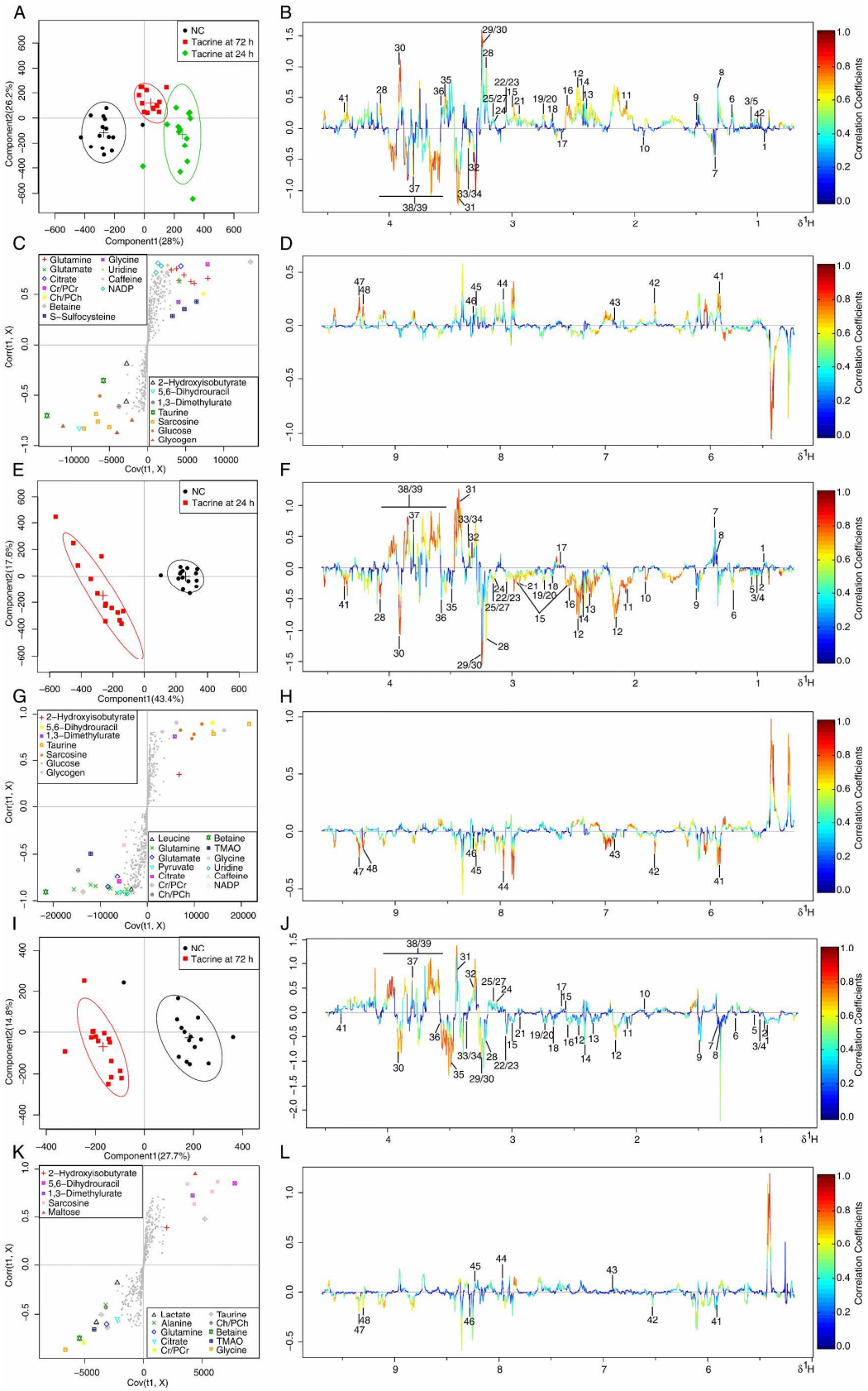

Fig. 7 Scores plots, S-plots and color-coded loading plots according to OSC-PLSDA analysis of

NMR data from liver extracts of rats: (A) Scores plot of three groups: NC, Tacrine at 24 and 72 h; (C) S-plot of three groups: NC, Tacrine at 24 and 72 h; (B and D) color-coded loading plots from OSC-PLSDA analysis showed the metabolite components that differed between the three groups: NC, Tacrine at 24 and 72 h; (E) Scores plot of two groups: NC and Tacrine at 24 h; (G) S-plot of two groups: NC and Tacrine at 24 h; (F and H) color-coded loading plots showed the metabolite components that differed between the two groups: NC and Tacrine at 24 h; (I) Scores plot of two groups: NC and Tacrine at 72 h; (K) S-plot of two groups: NC and Tacrine at 72 h; (J and L) color-coded loading plots showed the metabolite components that differed between the two groups: NC and Tacrine at 72 h.

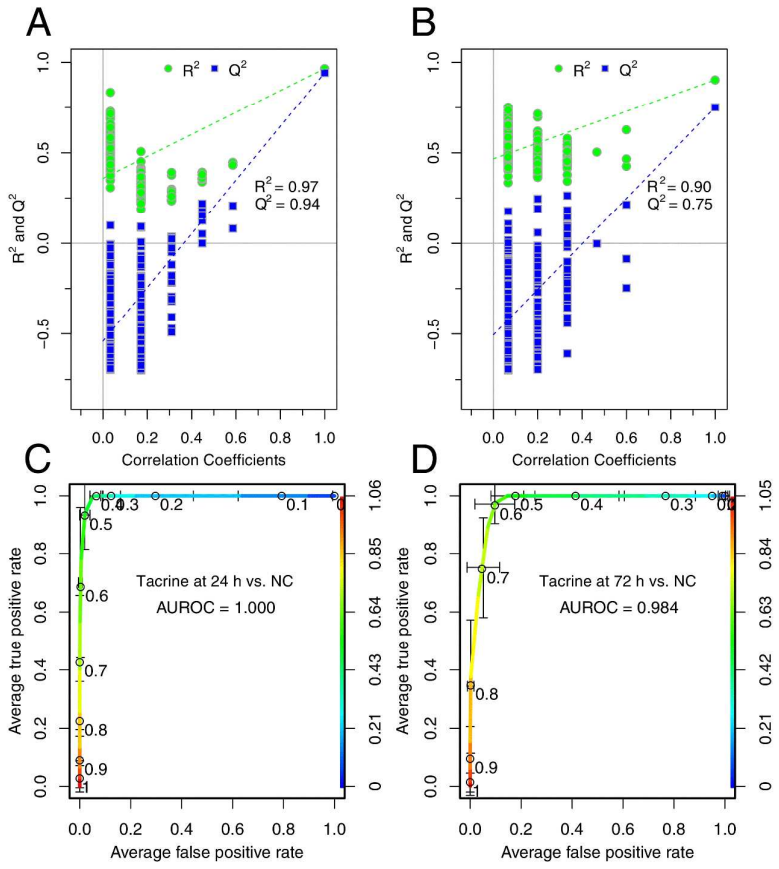

Fig. 8 OSC-PLSDA scatter plots of statistical validation obtained by 200 times permutation test, with R^2 and Q^2 values in the *vertical axis*, the correlation coefficients (between the permuted and true class) in the *horizontal axis*, and the OLS line for the regression of R^2 and Q^2 on the correlation coefficients. (A) *Y*-axis intercepts: R^2 = (0.0, 0.359), Q^2 = (0.0, -0.541) for the NC

group and the 24 h tacrine treated group; (B) *Y*-axis intercepts: R^2 = (0.0, 0.467), Q^2 = (0.0, -0.506) for the NC group and the 72 h tacrine treated group. (C, D) Receiver operating characteristic (ROC) curves of classifier performance of OSC-PLSDA models on ^{1}H NMR data of the NC group and the 24 h tacrine treated group, the NC group and the 72 h tacrine treated group. The *x*-axis denotes the false positive rate, and the *y*-axis denotes the true positive rate. After repeated 2-fold cross-validation 20 times, the area under the ROC curve (AUROC) was calculated.

3.6 Univariate analysis

Parametric (*t* test) and non-parametric statistical tests (Wilcoxon signed rank test) were performed to assess important metabolites that were increased or decreased between the groups using R. The areas of metabolites were first tested for normality of the distribution. If the distribution followed the normality assumption, a parametric Student's *t*-test was applied; otherwise, a nonparametric (Mann–Whitney test) test was performed to detect statistically significant metabolites. The fold change values of metabolites between groups were calculated and the associated *P*-values were adjusted by the Benjamini & Hochberg (BH) method[35] for controlling the false positive rate in multiple comparisons using scripts written in R language. The results were listed in Table 2.

Table 2 Assignments of NMR signals for endogenous metabolites, their fold change values (Tacrine at 24 h group vs. NC and Tacrine at 72 h group vs. NC) and associated *P*-values.

Metabolite	Assignments	Chemical shift (ppm)	24 hr vs. NC		72 hr vs. NC	
			FC	*P*	FC	*P*
Isoleucine	δCH_3, γCH_3, γCH_2	0.93(t), 1.00(d), 1.46(m)	0.98		0.78	
Leucine	δCH_3, δCH_3, γCH, αCH_2	0.96(t), 0.97(t), 1.70(m), 3.73(m)	0.78	*	0.89	
Valine	γCH_3, γCH_3, βCH, αCH	0.99(d), 1.05(d), 2.26(m), 3.60(d)	1.04		0.96	

Isobutyrate	βCH_3, αCH	1.05(d), 2.38(q)	0.84		0.98		
3-Hydroxybutyrate	γCH_3, αCH_2, βCH	1.21(d), 2.30(dd), 2.39(dd), 4.14(m)	0.77	*	1.12		
Lactate	βCH_3, αCH	1.34(d), 4.11(q)	1.00		0.93		
2-Hydroxyisobutyrate	CH_3	1.35(s)	1.18	*	0.95		
Alanine	βCH_3, αCH	1.49(d), 3.78(q)	0.99		0.94		
Acetate	CH_3	1.93(s)	0.59	***	1.02		
Glutamine	βCH_2, γCH_2, αCH	2.16(m), 2.46(m), 3.77(t)	0.61	***	0.90		
Butanone	βCH_3, αCH_3, αCH_2	0.99(t), 2.18(s), 2.57(q)	0.90	**	0.95		
Glutamate	βCH_2, γCH_2, αCH	2.04(m), 2.12(m), 2.34(m), 3.75(m)	0.64	***	0.96		
Pyruvate	βCH_3	2.36(s)	0.55	***	0.95		
Succinate	CH_2	2.39(s)	0.52	***	1.20		
Isocitrate	$1/2CH_2$, $1/2CH_2$	2.49(AB), 2.59(AB)	0.78	***	0.85		
β-Alanine	αCH_2, βCH_2	2.54(t), 3.18(t)	1.22		1.74		
Methylamino	CH_3	2.61(s)	1.05		0.97		
5,6-Dihydrouracil	5-CH_2, 6-CH_2	2.66(t), 3.45(t)	1.34	***	1.25	**	
Sarcosine	CH_3, CH_2	2.73(s), 3.60(s)	1.85	**	1.11		
Dimethylamino	CH_3	2.72(s)	0.88		0.90		
N-Methylhydantoin	N-CH_3, CH_2	2.94(s), 4.08(s)	0.32	***	1.52		
Cr/PCr	CH_3, CH_2	3.02(s), 3.92(s)	0.84	***	0.97		
Creatinine	CH_3, CH_2	3.04(s), 4.05(s)	0.73	***	0.84		
Malonate	CH_2	3.12(s)	1.08		1.27		
Ethanolamino	NH-CH_2, OH-CH_2	3.15(t), 3.81(t)	0.82	*	1.31		
N-Nitrosodimethylamine	CH_3	3.15(s)	1.05		0.97		
Ch/PCh	$N(CH_3)_3$, N-CH_2, OCH_2	3.19(s), 3.51(m), 4.06(s)	0.57	*	0.93		
Betaine	CH_3, CH_2	3.25(s), 3.89(s)	0.60	***	0.94		
TMAO	CH_3	3.25(s)	0.96		1.01		
Taurine	SO_3-CH_2, CH_2-NH_2	3.27(t), 3.43(t)	1.27	**	1.02		
1,3-Dimethylurate	3-CH_3, 1-CH_3	3.30(s), 3.44(s)	1.44	**	1.31		
Caffeine	1-CH_3, 3-CH_3, 7-CH_3, 8-CH	3.34(s), 3.52(s), 3.94(s), 7.90(s)	0.63	***	0.97		
Methanol	CH_3	3.37(s)	1.08		1.98		
S-Sulfocysteine	βCH_2, αCH	3.50(dd), 3.67(dd), 4.19(t)	0.91		0.92		
Glycine	CH_2	3.56(s)	0.95	*	0.96		
Guanidoacetate	CH_2	3.79(s)	1.03		0.94		
Glucose		3.23(t), 5.25(d)	1.28	**	1.31	*	
Glycogen		5.4	3.37	***	1.52	**	
Phenylalanine	CH=CH, CH_2, CH-NH_2	3.12(m), 3.28(m), 3.99(t), 7.34(d), 7.38(dd), 7.43(m)	0.99		1.11		
Uridine	5-CH, 1'-CH, 6-CH	5.89(d), 5.91(d), 7.86(d)	0.60	***	0.93		
Fumarate	CH=CH	6.51(s)	0.99		0.93		
Protocatechuate	5-CH, 2-CH, 6-CH	6.91(d), 7.37(d), 7.39(m)	0.86	*	1.12		
Xanthine	CH	7.90(s)	2.24	**	0.92		
Hypoxanthine	2CH, 8CH	8.18(s), 8.20(s)	0.94		0.91		
Oxypurinol	CH	8.22(s)	0.69	**	1.20		
NAD	7-CH, 39-CH, 7-CH, 38-CH, 12-CH, 28-CH, 2-CH	9.33(s), 9.14(d), 8.84(d), 8.41(s), 8.19(t), 8.16(t), 6.09(d), 6.03(d)	0.54	**	0.59	***	
NADP	35-CH, 37-CH, 39-CH, 7-CH, 38-CH, 12-CH, 28-CH, 2-CH	9.29(s), 9.10(d), 8.82(d), 8.41(s), 8.18(t), 8.14(t), 6.10(d), 6.04(d)	0.49	***	0.63	***	

Multiplicity: s singlet, d doublet, t triplet, dd doublet of doublets, q quarters, m multiplet. Color coded according to $\log_2$ (Fold Change) using color bar 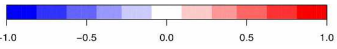

$^*P <$ 0.05, $^{**}P < 0.01$ and $^{***}P < 0.001$ for Tacrine at 24 h group vs. NC and Tacrine at 72 h group vs. NC.

Cr/PCr: Creatine/Phosphocreatine; Ch/PCh: Choline/Phosphocholine; TMAO: Trimethylamine *N*-oxide

4 Discussion

In this study, histopathology, clinical chemistry and the mRNA expressions of related enzymes were applied to investigate the metabolic events in the liver by tacrine treatment. Histopathological inspection revealed severe liver impairments induced by tacrine, which was evidenced by increased levels of AST and ALT in blood and MDA, GSH in liver, and a decreased level of total proteins in liver.

To investigate the variations of endogenous metabolites in rats administered with tacrine, a ^{1}H NMR-based metabolomics approach was adopted to explore potential biomarkers and the affected metabolic pathways. The pathway analysis revealed that the most affected metabolic disturbance by tacrine treatment was energy metabolism in TCA cycle, glycolysis or gluconeogenesis. In addition, metabolisms of pyruvate; nicotinate and nicotinamide; alanine, aspartate and glutamate; taurine and hypotaurine and D-glutamine and D-glutamate were also disturbed by tacrine (Fig. 9). A schematic diagram of the perturbed metabolic pathways is shown in Fig. 10.

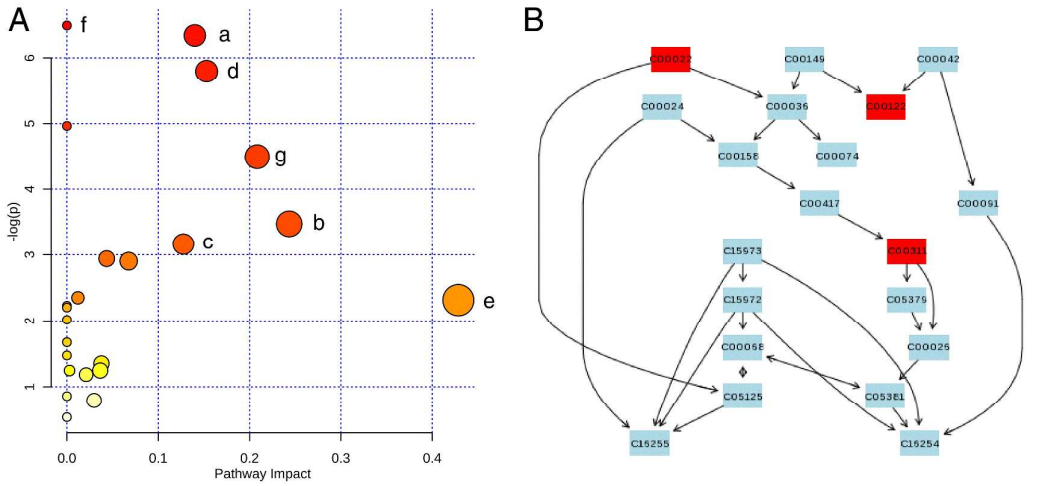

Fig. 9 Overview of altered metabolism pathways in liver tissues (A) of tacrine treated rats at 24 and 72 h compared with control rats as visualized by bubble plots. Bubble area is proportional to the impact of each pathway, with color denoting the significance from highest in red to lowest in white. ((a) TCA cycle; (b) pyruvate metabolism; (c) glycolysis or gluconeogenesis; (d) alanine, aspartate and glutamate metabolism; (e) taurine and hypotaurine metabolism; (f) D-glutamine and D-glutamate metabolism; (g) nicotinate and nicotinamide metabolism. (B) The pathway flowchart of the most impacted is TCA cycle.

4.1 Energy metabolism

The major source of energy supply is the oxidation of glucose to produce ATP through the TCA cycle *via* mitochondrial respiratory chain. One glucose molecule breaks down into two pyruvates by glycolysis. Pyruvate can produce acetyl-CoA, which enters into the TCA cycle, promoting the conversion from NAD^+ to NADH that is used in the respiratory chain.[36] To produce ATPs, the electrons carried by NADH pass throughout the electron transport chain to O_2 in mitochondria, which is carried out by four inner-membrane-associated enzyme complexes, namely NADH: ubiquinone oxidoreductase (complex I), succinate: ubiquinone oxidoreductase

(complex II), ubiquinol: ferricytochrome C oxidoreductase (complex III) and ferrocytochrome C: oxygen oxidoreductase (complex IV).[37] At the same time, protons are pumped out of the mitochondria into the cytoplasm, which makes the interior of the mitochondria alkaline, thus forming a pH gradient. The existence of such a pH gradient helps the inflow of protons into the mitochondria through the action of ATP synthase, which is then activated and catalyzes the production of ATP from ADP and Pi. Tacrine, by its free and protonated forms, has been reported to have the ability to shuttle across the inner mitochondrial membrane with protons. Therefore, tacrine destroys the proton gradient and hampers the production of ATP. Insufficient ATP generation leads to mitochondrial dysfunction or even to cell death depending on the dosage of tacrine.[16,38] To regain the pH gradient and the level of ATP, the body had to accelerate respiratory chain reaction by consumption of NADH to pump protons out of the inner mitochondrial membrane, which was evidenced by the upregulated hepatic expressions of respiratory chain Complex I and II genes at 24 h after tacrine administration and the markedly increased level of its product NAD^+. Unfortunately, this process itself consumed ATP, which was evidenced by significantly increased levels of its two products, hypoxanthine and xanthine,[39] at 24 h after tacrine treatment.

To survive this energy crisis, at least two alternative means were adopted in tacrine treated rats. One was the oxidation of fatty acids, oxidized first to 3-hydroxybutyrate and finally to acetate, producing ATP at the same time.[40] The significant increases of 3-hydroxybutyrate and acetate at 24 h in livers of rats treated with tacrine suggested an accelerated oxidation of fatty acids. The inefficient energy

supply called for another mean by more utilization of glucose and its reservoir, glycogen. As a result, levels of liver glucose and glycogen were significantly decreased at 24 and 72 h, which were consistent with those observed in hepatic cells treated with tacrine.[41] Glycogen phosphorylase catalyzes the rate-limiting step in glycogenolysis and sets the upper limit for the rates of glycolysis.[42] The expression of glycogen phosphorylase gene was significantly increased at 24 h confirming an accelerated glycogenolysis. The consumption of glucose and glycogen *via* glycolysis and glycogenolysis would produce pyruvate, which was increased in the liver of rats treated with tacrine at 24 h after dosing. The activity of pyruvate kinase (the key enzyme for glycolysis) of treated rats at 24 and 72 h after dosing was significantly augmented, demonstrating an enhanced glycolysis induced by tacrine. Pyruvate could be degraded to form acetyl-CoA entering into TCA cycle. TCA cycle was accelerated after tacrine dosing, as evidenced by the elevated levels of isocitrate, succinate and fumarate (intermediates of the TCA cycle). Citrate synthase is the first enzyme of the TCA cycle and thus is a key regulator of TCA cycle rate and intracellular ATP production in both prokaryotic and eucaryotic cells.[43] Another rate-controlling enzyme in the TCA cycle is α-ketoglutarate dehydrogenase. The hepatic expressions of citrate synthase and α-ketoglutarate dehydrogenase genes were all increased at 24 h after tacrine treatment, thus confirming a promoted TCA cycle by tacrine.

Creatine, phosphocreatine and creatinine, through the creatine kinase reaction, play an important role in maintaining a constant ATP level.[44] Creatine is synthesized and metabolized in the liver, with the kidney providing the necessary synthetic

464 precursor. When the body was in shortage of ATP, phosphocreatine would be
465 catalyzed by creatine kinase to form ATP. Significant increases of creatine, creatintine
466 and augmentation in the activity of creatine kinase in the liver of rats administrated
467 with tacrine suggested an accelerated utilization of phosphocreatine to meet the
468 energy demand.
469

470 **4.2 Oxidative stress**

471 It is reported that tacrine could reduce the level of GSH in rat hepatocytes,[41] and
472 induce ROS production in living cells.[45] In this study, GSH was indeed slightly
473 decreased at 24 h after tacrine treatment by clinical chemistry. As the most abundant
474 natural antioxidant in mammalian tissues, GSH shows a variety of physiological
475 functions, including xenobiotic detoxification and antioxidant defense.[46] The
476 depletion of GSH suggested a status of oxidative stress, which was also supported by
477 the markedly ever-increasing of MDA after the administration of tacrine. To replenish
478 the greatly consumed GSH, the body had to markedly facilitate its synthesis, which
479 could be evidenced by the significantly increased levels of its two precursors,
480 glutamine and glutamate in livers[47] of tacrine treated rats at 24 h. This effort led to a
481 huge amount of GSH production and a marked increase at 72 h, at the expense of a
482 great consumption of glutamine and glutamate, which were observed with significant
483 increases at 24 h but no obvious alteration at 72 h. Glutathione synthetase can
484 catalyze the ATP-dependent synthesis of GSH from gamma-glutamylcysteine (which
485 is synthesized from glutamate) and glycine.[48] The expression of glutathione

synthetase gene was increased at 24 h and decreased at 72 h, and therefore, further demonstrated an accelerated GSH synthesis at 24 h and an inhibition of its synthesis at 72 h. Besides GSH, other antioxidants also helped the body counteract oxidative stress, such as taurine, which was significantly decreased in liver of tacrine dosed rats both at 24 and 72 h. Taurine is a major free intracellular amino acid found in many animal tissues with various important properties such as antioxidant and anti-apoptotic activities and the abilities to protect against hepatic damage and regulate osmotic pressure, ion transport and DNA repair.[49,50]

Cell membrane lipids, rich in poly unsaturated fatty acids, are especially sensitive to oxidative damage.[51] ROS induced oxidative damage of phospholipids, posing a severe menace to the viability of the cells. ROS disrupted both the construction and function of cell membranes, eventually resulting in the rupture of cells and organelles, such as mitochondria.[52] Phospholipids are essential components of the cell membranes. Synthesized *in vivo* or obtained by food intake, choline and phosphocholine are the main components of phospholipids. The levels of choline and phosphocholine in the livers of drug treated rats were significant increase, suggesting disruption of cell membrane.[23] Hence, the elevation of choline and phosphocholine could be signs for tacrine-induced cell and mitochondrial membrane damage.

Besides lipids, DNAs and RNAs were also susceptible to oxidative damage,[53] which was evidenced by significant increase of uridine in the livers of tacrine treated rats at 24 h. As a component of RNA, uridine can be catalyzed by thymidilate synthase to form thymidine which is incorporated into DNA. Tacrine impaired DNA

polymerase γ-mediated DNA replication and also poisoned topoisomerases I and II to increase the relaxation of a supercoiled plasmid *in vitro*. Tacrine markedly decreased the incorporation of thymidine into mitochondrial DNA (mtDNA) encoding several protein subunits involved in the electron transport, thus progressively and severely depleted mtDNA.[54,55]

Proteins are another target of oxidative damage, leading to changes in the three-dimensional structure of proteins and even to their fragmentation.[56] The total proteins were markedly decreased at 24 and 72 h, suggesting a severe protein damage by tacrine, in consistent with the findings in hepatic cells treated with tacrine.[37]

In conclusion, mitochondria are crucial for energy production and metabolism as the TCA cycle and respiratory chain are located in the mitochondrial matrix. Mitochondria play a key role in the maintenance of metabolic homeostasis and activation of necessary stress responses.[54] Tacrine destroyed the proton gradient of mitochondria and hampered the production of ATP, which led to mitochondrial dysfunction. To regain the disrupted proton gradient, the body had to accelerate the respiratory chain reaction and TCA cycle. In response to a status of energy shortage induced by tacrine, enhanced oxidation of fatty acids and accelerated utilization of glucose and its reservoir, glycogen were observed in tacrine dosed rats. Therefore, the broken proton gradient induced mitochondrial dysfunction and energy metabolism disturbance. Mitochondria were believed to be one of the major factories of ROS during respiratory metabolism.[57] The disordered mitochondria released additional ROS, thus inducing oxidative stress which caused cell membrane damage, and

proteins degradation, mitochondrial DNA rupture. As a result, severe mitochondrial destruction and cell damage amplified the oxidative damage to cause cell death, which might be the major mechanism underlying the hepatotoxicity of tacrine.

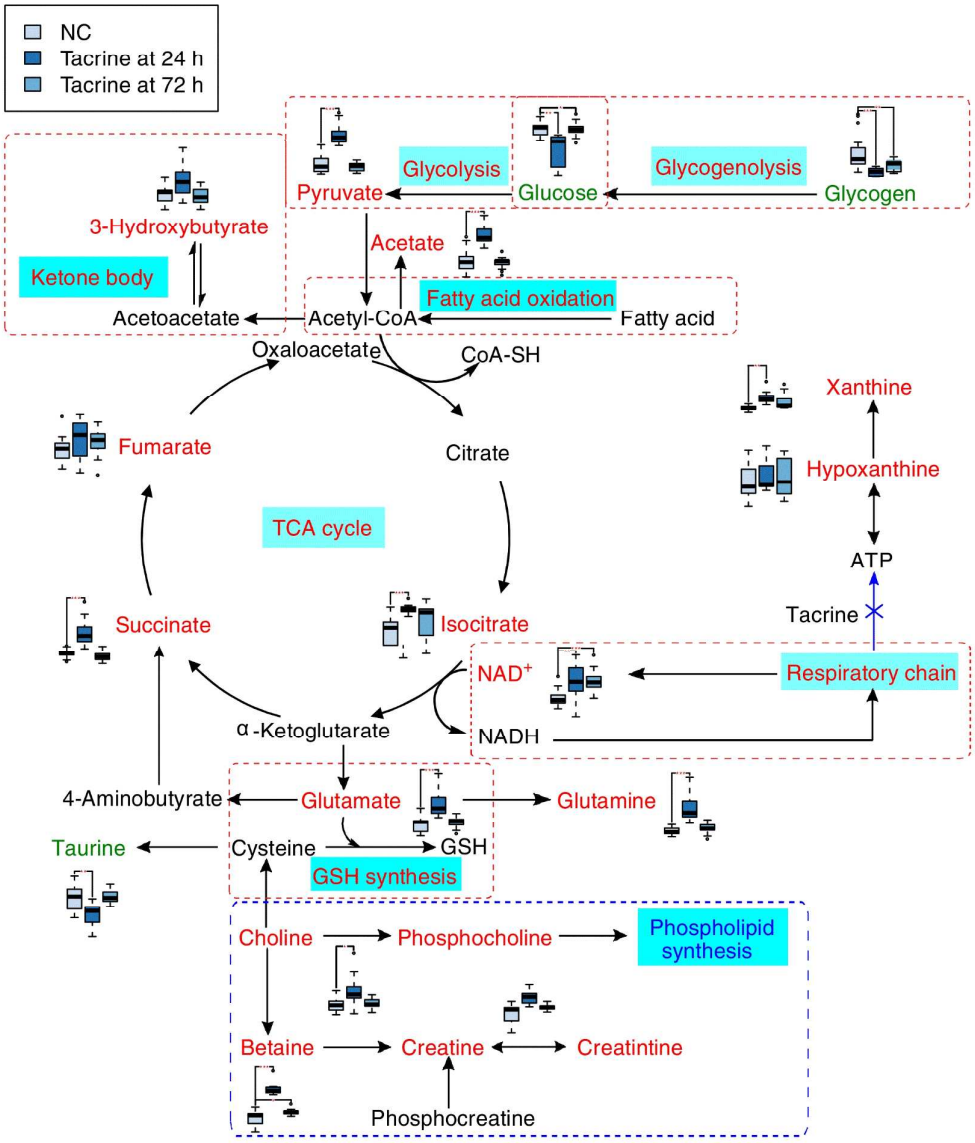

Fig. 10 Schematic illustrating the major perturbed metabolic pathways in tacrine treated rats detected by ^{1}H NMR analysis. Identified metabolic pathways were marked in light blue rectangle. The words in dark blue mean inhibited pathways, words in red mean promoted pathways. TCA cycle and respiratory chain were the junction pathways of energy metabolism and lipid metabolism. Metabolites in red and green represent the notable increase and decrease, respectively.

Metabolites in black mean they were not detected. The metabolites in control, 24 and 72 h after tacrine treatment groups for all time-point are presented by box-plots. Symbols '○' are used as the outliers. *P < 0.05, **P <0.01 and ***P < 0.001 for tacrine treated groups vs. NC at all time-point.

5 Conclusion

Metabolomics is a novel holistic approach that promises to enable the discovery of pathways of complex diseases and exploration of the dynamic process of drug induced toxicity. ^{1}H NMR-based metabolomics approach combined with histopathological inspection and clinical chemistry assays was applied for the first time to study the acute toxicity of tacrine. Tacrine induced perturbations in energy metabolism and oxidative stress producing a series of damage. These findings helped to explain the tacrine-induced hepatotoxicity and provided several potential biomarkers denoting its toxicity.

6 Acknowledgements

This research work was financially supported by the Key Project of National Natural Science Foundation of China (81430092), NSFC grant 81173526, the Program for New Century Excellent Talents in University (NCET-11-0738), and the Program for Changjiang Scholars and Innovative Research Team in University (PCSIRT-IRT1193).

Reference

1. N. J. Owens, *Hosp. Formul.*, 1993, **28**, 679-691.

2. C. Starr, *Drug Topics*, 1992, **14**, 32-42.
3. B. W. Volger, *Clin. Pharmacokinet*., 1991, **10**, 447-456.
4. M. Farlow, S. I. Gracon, L. A. Hershey, K. W. Lewis, C. H. Salowsky, J. Dolan-Ureno, *J. Am. Med. Assoc*., 1992, **268**, 2523-2529.
5. M. J. Knapp, D. S. Knopman, P. R. Solomon, W. W. Pendlebury, C. S. Davis, S. I. Gracon, *J. Am. Med. Assoc*., 1994, **271**, 985-991.
6. C. S. Wu and J. T. Yang, *Mol. Pharmacol*., 1989, **35**, 85-92.
7. A. J. Hunter, T. K. Murray, J. A. Jones, A. J. Cross and A. R. Green, *Brit. J. Pharmacol*., 1989, **98**, 79-86.
8. K. L. Davis, Peter Powchik, *Lancet*, 1995, **345**, 625-630.
9. P. B. Watkins, H. J. Zimmerman, M. J. Knapp, S. I. Gracon, K. W. Lewis, *J. Am. Med. Assoc*., 1994, **271**, 992-998.
10. D. R. Forsyth, D. J. Sormon, R. A. Morgan, G. K. Wilcock, *Age Ageing*, 1989, **18**, 223-229.
11. J. T. O'Brien, S. Eagger, R. Levy, *Age Ageing*, 1991, **20**, 129-131.
12. P. B. Watkins, H. J. Zimmerman, M. J. Knapp, S. I. Gracon, K. W. Lewis, *J. Am. Med. Assoc*., 1994, **271**, 992-998.
13. S. Madden, T. F. Woolf, W. F. Pool, B. K. Park, *Biochem. Pharmacol*., 1993, **46**, 13-20.
14. V. Spaldin, S. Madden, W. F. Pool, T. F. Woolf, B. K. Park, *Brit. J. Clin. Pharmaco*., 1994, **38**, 15-22.
15. C. J. Viau, R. O. Curren, K. Wallace, *Drug Chem. Toxicol*., 1993, **16**, 227-239.
16. A. Berson, S. Renault, P. Lettéron, M. A. Robin, B. Fromenty, D. Fau, M. A. Le Bot, C. Riche, A. M. Durand-Schneider, G. Feldmann, D. Pessayre, *Gastroenterology*, 1996, **110**, 1878-1890.
17. G. Feuee, F. A. Iglesia, *Drug-Induced Hepatotoxicity*, 1996, **121**, 447-513.
18. L. Suter, L. E. Babiss and E. B. Wheeldon, *Chem. Biol*., 2004, **11**, 161-171.
19. S. Ekins, Y. Nikolsky and T. Nikolskaya, *Trends Pharmacol. Sci.*, 2005, **26**, 202-209.
20. J. K. Nicholson, J. Connelly, J. C. Lindon and E. Holmes, *Nat. Rev. Drug Discov*., 2002, **1**, 153-162.
21. M. R. Viant, E. S. Rosenblum, R. S. Tjeerdema, *Environ. Sci. Technol*., 2003, **37**, 4982-4989.
22. J. P. Shockcor, E. Holmes, *Curr. Top. Med. Chem*., 2005, **17**, 121-147.
23. J. L. Griffin, *Drug Discovery Today: Technologies*, 2004, **1**, 285-293.
24. L. Li, B. Sun, Q. Zhang, J. Fang, K. Ma, Y. Li, H. Chen, F. Dong, Y. Gao, F. Li and X. Yan, *J. Ethnopharmacol.*, 2008, **116**, 561-568.
25. C. Deback, J Géli, Z Aït-Arkoub, F Angleraud, A Gautheret-Dejean, H Agut and D Boutolleau, *J. Virol. Methods*, 2009, **159**, 291-294.
26. F. Dieterle, A. Ross, G. Schlotterbeck and H. Senn, *Anal. Chem*., 2006, **78**, 4281-4290.
27. J. A. Westerhuis, H. C. J. Hoefsloot, S. Smit, D. J. Vis, A. K. Smilde, E. J. J. van Velzen, J. P. M. van Duijnhoven, F. A. van Dorsten, *Metabolomics*, 2008, **4**, 81-89.
28. S. Bijlsma, L. Bobeldijk, E. R. Verheij, R. Ramaker, S. Kochhar, I. A. Macdonald, B. van Ommen, A. K. Smilde, *Anal. Chem*., 2006, **78**, 567-574.
29. J. G. Xia, N. Psychogios, N. Young, D. S. Wishart, *Nucleic Acids Res*., 2009, **37**, 652-660.
30. T. Sing, O. Sander, N. Beerenwinkel and T. Lengauer, *Bioinformatics*, 2005, **21**, 3940-3941.
31. O. Cloarec, M. E. Dumas, A. Craig, R. H. Barton, J. Trygg, J. Hudson, C. Blancher, D. Gauguier, J. C. Lindon, E. Holmes, *Anal. Chem*., 2005, **77**, 1282-1289.
32. J. Xia, R. Mandal, I. V. Sinelnikov, D. Broadhurst, D. S. Wishart, *Nucleic Acids Res*., 2012, **40**,

W127-W133.
33. K. J. Lee, J. H. Choi, H. G. Kim, E. H. Han, Y. P. Hwang, Y. C. Lee, Y. C. Chung, H. G. Jeong, *Food Chem. Toxicol*., 2008, **46**, 1778-1785.
34. M. S. Jurica, A. Mesecar, P. J. Heath, W. Shi, T. Nowak and B. L. Stoddard, *Structure*, 1998, **6**, 195-210.
35. Y. Benjamini, Y. Hochberg, *J. Roy. Stat. Soc. B*., 1995, **57**, 289-300.
36. H. Krebs, *Adv. Enzyme Regul*., 1970, **8**, 335-353.
37. H. Weiss, T. Friedrich, G. Hofhaus and D. Preis, *Eur. J. Biochem*., 1991, **197**, 563-576.
38. A. N. Murphy, G. Fiskum, M. F. Beal, *J. Cereb. Blood F. Met*., 1999, **19**, 231-245.
39. C. Barsotti, P. L. Ipata, *Int. J. Biochem. Cell B*., 2004, **36**, 2214-2225.
40. J. D. McGarry, D. W. Foster, *Annu. Rev Biochem*., 1980, **49**, 395-420.
41. D. Lagadic-Gossmann, M. Rissel, M. A. Le Bot and A. Guillouzo, *Cell Biol. Toxicol*., 1998, **14**, 361-373.
42. M. L. Parolin, A. Chesley, M. P. Matsos, L. L. Spriet, N. L. Jones and G. J. F. Heigenhauser, *Am. J. Physiol - Endoc M*., 1999, **277**, E890-900.
43. G. Wiegand, and S. J. Remington, *Annu. Rev. Biophys. Biophys. Chem*., 1986, **15**, 97-117.
44. H. J. Chen, Y. C. Shen, C. Y. Lin, K. C. Tsai, C. K. Lu, C. C. Shen and Y. L. Lin, *Metabolomics*, 2012, **8**, 974-984.
45. R. A. Osseni, C. Debbasch, M. O. Christen, P. Rat and J. M. Warnet, *Toxicol. In Vitro*, 1999, **13**, 683-688.
46. C. K. Sen, *J. Nutr. Biochem*., 1997, **8**, 660-672.
47. S. Hlais, D. R. Reslan, H. K. Sarieddine, L. Nasreddine, G. Taan, S. Azar, O. A. Obeid, *Clin. Ther*., 2012, **34**, 1674-1682.
48. C. M. Grant, F. H. MacIver and I. W. Dawes, *Mol. Biol. Cell*, 1997, **8**, 1699-1707.
49. V. V. Kuzmina, L. K. Gavrovskaya, O. V. Ryzhova, *J. Evol. Biochem. Phys.*, 2010, **46**, 19-27.
50. L. M. Jiang, J. Huang, Y. Wang, H. Tang, *J. Proteome Res*., 2012, **11**, 3848-3859.
51. J. W. Schmidley, *Stroke*, 1990, **21**, 1086-1090.
52. S. C. Smart, G. B. Fox, K. L. Allen, A. G. Swanson, M. J. Newman, G. T. G. Swayne, J. B. Clark, K. D. Sales and S. C. R. Williams, *NMR Biomed*., 1994, **7**, 356-365.
53. F. I. Milagro, J. Campión and J. A. Martínez, *Obesity*, 2006, **14**, 1118-1123.
54. A. Mansouri, D. Haouzi, V. Descatoire, C. Demeilliers, A. Sutton, N. Vadrot, B. Fromenty, G. Feldmann, D. Pessayre and A. Berson, *Hepatology*, 2003, **38**, 715-725.
55. E. Verdin, M. D. Hirschey, L. W. S. Finley and M. C. Haigis, *Trends Biochem. Sci*., 2010, **35**, 669-675.
56. M. H. Li, J. S. Wang, Z. G. Lu, D. D. Wei, M. H. Yang, L. Y. Kong, *Aquat. Toxicol*., 2014, **146**, 82-92.
57. L. Bambrick, T. Kristian, G. Fiskum, *Neurochem. Res.*, 2004, **29**, 601-608.

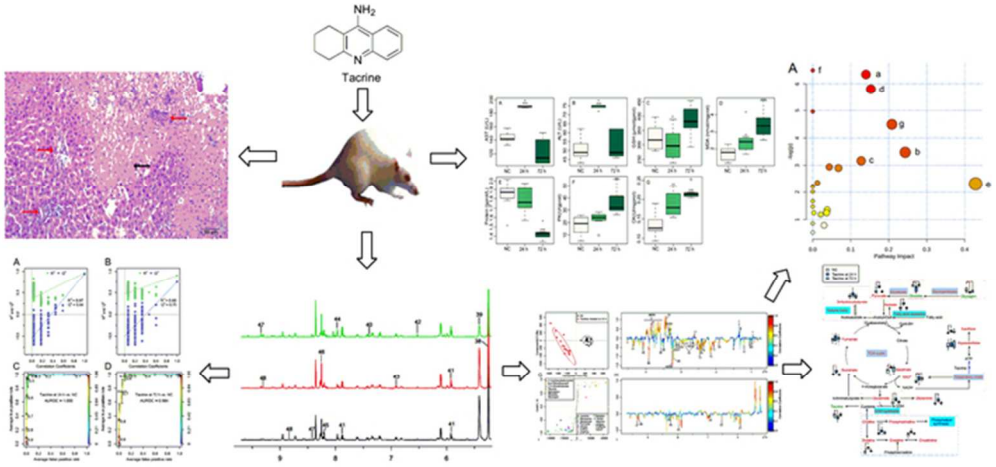

60x28mm (300 x 300 DPI)